

Circumstellar habitable zones for deep terrestrial biospheres

Sean McMahon^{1*}, Jack O'Malley-James², John Parnell¹

¹ School of Geosciences, University of Aberdeen, Meston Building, King's College, Aberdeen, AB24 3UE. * Corresponding author: sean.mcmahon@abdn.ac.uk (+44) 1224 273433

² School of Physics & Astronomy, University of St Andrews, North Haugh, St Andrews, Fife, KY16 9SS

Abstract

1 The *habitable zone* (HZ) is conventionally the thin shell of space around a star within which
2 liquid water is thermally stable on the surface of an Earth-like planet (Kasting et al., 1993).
3 However, life on Earth is not restricted to the surface and includes a “deep biosphere” reaching
4 several km in depth. Similarly, subsurface liquid water maintained by internal planetary heat
5 could potentially support life well outside conventional HZs. We introduce a new term,
6 *subsurface-habitability zone* (SSHZ) to denote the range of distances from a star within which
7 rocky planets are habitable at any depth below their surfaces up to a stipulated maximum, and
8 show how SSHZs can be estimated from a model relating temperature, depth and orbital
9 distance. We present results for Earth-like, Mars-like and selected extrasolar terrestrial planets,
10 and conclude that SSHZs are several times wider and include many more planets than
11 conventional surface-based habitable zones.

12 **Keywords:** habitable zone, deep biosphere, subsurface, astrobiology, exobiology, extrasolar
13 planets

1
2
3
4
5
6
7
8
9
10
11
12
13
14
15
16
17
18
19
20
21
22
23
24
25
26
27
28
29
30
31
32
33
34
35
36
37
38
39
40
41
42
43
44
45
46
47
48
49
50
51
52
53
54
55
56
57
58
59
60
61
62
63
64
65

15 **1. Introduction**

16

17 *1.1 Habitable zones and deep biospheres*

18 The concept of a circumstellar habitable zone (HZ) was formalised by Kasting et al. (1993) and
19 is widely employed in the planetary sciences. Within the conventional HZ, global average
20 planetary surface temperatures—buffered by a CO₂ weathering cycle—fall between the limits of
21 runaway greenhouse warming at the inner edge and runaway cooling driven by CO₂
22 condensation at the outer edge. Outside these limits, planetary surfaces are thought to be unable
23 to sustain liquid water and therefore life. In our own solar system, however, some of the most
24 promising candidates for habitable extraterrestrial environments are in the subsurface of planets
25 and moons outside the conventional HZ, such as Mars and Jupiter’s moon Europa (e.g. Boston et
26 al., 1992; Fisk and Giovannoni, 1999; Gaidos et al., 1999).

27

28 It has long been recognised that subsurface life on Earth provides a model for understanding how
29 life could adapt to conditions deep within a colder rocky planetary body (e.g. Gold, 1992).
30 Micro-organisms inhabit pores and fractures at depths of up to several km in the Earth’s crust,
31 constituting a “deep biosphere” with a total biomass that may be similar to the “surface
32 biosphere” (Whitman et al., 1998). Much of the deep biosphere relies on buried photosynthetic
33 organic matter and dissolved oxidants from the surface. However, some organisms
34 (chemolithoautotrophs) obtain nutrients and energy from geochemical sources that are largely
35 independent of surface conditions (Lin et al., 2006). Nutrients and redox couples for metabolism
36 are widespread in rocks, minerals and circulating fluids (e.g. Fisk and Giovannoni, 1998; Popa et
37 al., 2012). Hence, deep aquifers and hydrothermal systems in crystalline and sedimentary rocks

1
2
3
4 38 provide a habitable environment that could persist beyond the outer edge of the conventional
5
6 39 habitable zone. This scenario has been widely discussed in relation to Mars, where aquifers could
7
8
9 40 exist less than ten km below the surface (Travis et al., 2003). Similarly, many workers have
10
11 41 discussed whether Jupiter’s moons Europa, Callisto and Ganymede, Saturn’s moon Titan, and
12
13
14 42 other icy moons of the outer solar system may provide habitable conditions in deep oceans
15
16 43 beneath their outer ice shells (see Raulin et al., 2010 for review). Here, we extend the widely
17
18
19 44 used quantitative model of Kasting et al. (1993) for circumstellar habitable zones to include
20
21 45 terrestrial (rocky) planets with habitable temperatures in the subsurface down to a stipulated
22
23
24 46 depth. The possibility of adapting the model for icy bodies is also discussed.
25
26
27
28

29 48 *1.2 Subsurface-habitability zones*

30
31 49 We introduce a new term, “subsurface-habitability zone” (SSHZ) to denote the range of
32
33 50 distances from a star within which terrestrial planets are habitable at any depth below their
34
35
36 51 surfaces up to a certain maximum, z_{\max} (for instance, within the “SSHZ for 2 km depth”, planets
37
38 52 can support liquid water at a depth of 2 km or less). SSHZs directly extend the conventional
39
40
41 53 habitable zone, which is reproduced by setting z_{\max} equal to 0. In this paper, we show how
42
43 54 SSHZs can be estimated from a model of how the global average temperature (1) decreases with
44
45
46 55 increasing orbital distance, and (2) increases with depth in the crust.
47

48
49 56 The “habitable layer” is placed where global average temperatures fall between T_{\min} , the freezing
50
51 57 point of water, and T_{\max} , the upper limit of viability for known life, until the base is truncated by
52
53
54 58 z_{\max} (**Figure 1**). We find the thickness and depth of the habitable layer by coupling a
55
56 59 conventional model for planetary surface temperature (as a function of orbital distance) with a
57
58
59 60 geothermal gradient. The outer edge of the SSHZ is placed at the heliocentric distance where the
60
61
62
63
64
65

1
2
3
4 61 habitable layer pinches out at z_{\max} ; in other words, the temperature at z_{\max} passes below T_{\min} . The
5
6
7 62 inner edge of the SSHZ can be placed either where the average surface temperature reaches T_{\max} ,
8
9 63 or—because a planet too hot to maintain surface water would probably vent and lose subsurface
10
11
12 64 water on a geologically short timescale—at the conventional HZ inner edge. It should be noted
13
14 65 that both the conventional HZ and the SSHZ are determined by planetary average temperatures
15
16 66 although in reality temperature and other controls on habitability vary regionally (see *Section*
17
18
19 67 *4.1*).

22 68 *1.3 The maximum habitable depth*

25 69 If desired, the maximum depth (z_{\max}) can be used to represent a physical obstacle to deeper
26
27 70 infiltration by the biosphere. Fractures and pores are compacted under high lithostatic pressures
28
29
30 71 and occluded by secondary mineral growth. Thus, this obstacle could be a minimum threshold in
31
32
33 72 porosity, permeability or hydraulic connectivity. The upper pressure limit for known microbial
34
35 73 survival is on the order of GPa and is therefore unlikely to be encountered in pore water at a
36
37
38 74 shallower depth than these geophysical barriers or T_{\max} . (Sharma et al., 2002; Vanlint et al.,
39
40 75 2011). However, relationships between pressure, temperature, rock rheology, permeability,
41
42
43 76 porosity, fluid flow and other controls on habitability are not well constrained; on Earth, the
44
45 77 depth of penetration by the biosphere is probably limited by temperature (for discussion, see
46
47
48 78 Jones et al., 2011). A physically meaningful z_{\max} would be temperature-dependent and therefore
49
50 79 vary with orbital distance, potentially failing to truncate the habitable layer (as defined in *1.2*)
51
52
53 80 and hence to define an SSHZ outer edge. In any case, z_{\max} can be used more generally to limit a
54
55 81 depth range of interest; the SSHZ outer edge is simply the maximum orbital distance of a planet
56
57 82 habitable at that particular depth.
58
59
60
61
62
63
64
65

1
2
3
4
5
6
7
8
9
10
11
12
13
14
15
16
17
18
19
20
21
22
23
24
25
26
27
28
29
30
31
32
33
34
35
36
37
38
39
40
41
42
43
44
45
46
47
48
49
50
51
52
53
54
55
56
57
58
59
60
61
62
63
64
65

83

2. Methods

85

2.1 Surface temperature

87

Surface temperature, T_s , is estimated from the combined solar and geothermal heat flux on the assumption of thermal equilibrium at the surface of the planet (heat absorbed = heat emitted).

88

89

From the Stefan-Boltzmann law, the total heat radiated from the surface is given by $Q_{\text{total}} = 4\pi R^2 \epsilon \sigma T_s^4$, where R is the planetary radius, σ is the Stefan-Boltzmann constant, ϵ is emissivity and T_s is surface temperature. At equilibrium, $Q_{\text{total}} =$ internal heat (Q_{int}) + solar heat (Q_{sol}).

90

92 Solving for T_s :

91

$$T_s = \sqrt[4]{\frac{Q_{\text{int}} + Q_{\text{sol}}}{4\epsilon\sigma\pi R^2}}$$

93 (1)

94

95

Q_{sol} is equal to $(1 - a)\pi R^2 H_0$, where a is the planetary albedo and H_0 is the solar irradiance (power density) at the orbital distance of the planet. For Earth-like atmospheres, we modify T_s using simple temperature-dependent fluxes of the greenhouse gases H_2O and CO_2 . The partial optical thicknesses τ_{CO_2} and $\tau_{\text{H}_2\text{O}}$ are given by $0.029 \times \rho_{\text{CO}_2} T$ and $0.087 \times \rho_{\text{H}_2\text{O}} T$ respectively, where ρ_i is the partial pressure of gas i in the atmosphere, which is itself a function of temperature:

96

97

98

99

$$\rho_i = \frac{n_i RT}{N_A}$$

100 (2)

101

1
2
3
4 102 where n_i is the number density of the gas molecules in 1 m^3 of the atmosphere, R is the universal
5
6 103 gas constant and N_A is Avogadro's constant. The partial pressures of H_2O and CO_2 in the
7
8
9 104 atmosphere are accounted for following the conventions of Caldeira and Kasting (1992) and
10
11 105 Kasting et al. (1993), using the updated boundary conditions of Kopparapu et al. (2013).
12
13
14 106 Replacing T_{eff} , the effective temperature due to solar radiation (i.e. $(Q_{\text{sol}}/4\pi\epsilon\sigma R^2)^{1/4}$) with $T_{\text{eff}}(1 +$
15
16 107 $0.75\tau)^{1/4}$ gives a surface temperature that overshoots the actual value because it assumes a perfect
17
18
19 108 greenhouse. A final surface temperature is estimated by calculating the energy losses from the
20
21
22 109 system.

23
24
25 110 Q_{int} , the planetary internal heat, is assumed for simplicity to scale linearly with mass and is given
26
27 111 by $= (4/3)\pi R^3 \rho Q_M$, where Q_M is the heat production per unit mass and ρ is the bulk density.
28
29
30 112 Except when stated otherwise, Q_M and ρ were given terrestrial values ($7.4 \times 10^{12} \text{ W kg}^{-1}$ [Pollack
31
32 113 et al., 1993] and $5.515 \times 10^3 \text{ kg m}^{-3}$ respectively). The assumption that heat production scales
33
34
35 114 linearly with mass is justified if most heat production is radiogenic (whereas accretional heat
36
37 115 should scale with M^2/R [Selsis et al., 2008] and tidal heating depends on orbital configurations);
38
39
40 116 the relative contributions of the Earth's heat sources are currently poorly constrained.

41
42
43 117

44 118 *2.2 Habitable layers and SSHZs*

45
46 119 The flux of internal heat to the surface, q , is obtained by dividing Q_{int} by the surface area of the
47
48 120 planet. The increased lag time for internal heat to reach the surface of larger planets is not taken
49
50
51 121 into account; this increase may be small given that mantle convection rates are expected to scale
52
53
54 122 with $M^{1.19}$ (Valencia et al., 2007). A depth interval Δz corresponding to a temperature increase
55
56
57 123 $T_1 - T_0$ is found by:

$$\Delta z = \frac{\int_{T_0}^{T_1} K(T) dT}{q} \quad (3)$$

where $K(T)$ is the temperature-dependent thermal conductivity of the medium, assumed to be similar to basalt. We do not consider other influences on $K(T)$ such as pressure, rock porosity, water saturation, clathrates, ammonia or solutes in water. Since no data exist for $K(T)$ of basalt at very low temperatures, we follow Clifford et al. (2010) in approximating it by an empirical relation derived for water ice (Petrenko and Whitworth, 1999) which closely matches the $K(T)$ of basalt at higher temperatures. At 246 K, this function intersects the empirical relation of Clauser and Huenges (1995) for the thermal conductivity of basaltic rocks verified between 323 and 1273 K, which we therefore use for temperatures higher than 246 K. The use of these two relations together results in a smoothly continuous $K(T)$ curve for basalt throughout the desired temperature range. We thereby find both the top of the habitable layer and its base as a function of surface temperature and hence orbital distance.

The top of the habitable layer is placed at the shallowest depth where temperature is equal to or higher than T_{\min} . The base is placed at the depth of T_{\max} (395 K; Takai et al., 2008) except where that depth exceeds the stipulated maximum depth, z_{\max} , in which case the base is placed at z_{\max} . This allows the calculation of SSHZ inner and outer edges as noted in 1.2 and illustrated by Figure 1. As noted in 1.2, the inner edge of the SSHZ can be placed either where T_s reaches T_{\max} (the maximum temperature known to support life), or at the conventional HZ inner edge; for Earth-like atmospheres there is very little difference between these two values because of runaway global warming at the inner edge. The outer edge of the SSHZ is placed at the distance beyond which temperature does not exceed T_{\min} (the freezing point of water) at any depth

1
2
3
4 145 shallower than the chosen z_{\max} . Thus, any planet within the SSHZ can sustain liquid water at
5
6
7 146 some depth $\leq z_{\max}$.
8
9

10 147

13 148 **3. Results**

15
16 149

18 150 *3.1 General results*

21 151 SSHZs expand several-fold the range of heliocentric distances designated “habitable”. The
22
23
24 152 relationship between orbital distance and the position of the habitable layer is illustrated for the
25
26 153 most general case (i.e. with no atmospheric feedbacks) by **Figure 1**. In this example, the planet is
27
28 154 given Earth’s radius, bulk density, and estimated internal heat production, as well as a fixed
29
30 155 albedo and emissivity with Earth’s values. Because atmospheric feedbacks are not included, the
31
32
33
34 156 HZ and SSHZ are shifted towards the sun compared to a planet with an Earth-like atmosphere.
35
36

37 157 SSHZ outer-edge positions are highly sensitive to the maximum habitable depth, z_{\max} ; outer
38
39 158 edges for $z_{\max} = 5$ and 10 km are marked on Figure 1. In this example, the SSHZ is only limited
40
41
42 159 when z_{\max} is shallower than ~ 15.4 km (the asymptote in the top of the habitable layer). For higher
43
44 160 z_{\max} , SSHZs are unbounded; the planet’s internal heat production is such that subsurface
45
46 161 temperatures are within habitable limits even without additional heat from a star.
47
48
49

50 162 Higher albedos reduce surface temperature, shifting the habitable zone towards the star and
51
52 163 reducing its width (**Figure 2**). The effect on the SSHZ outer-edge position is stronger for higher
53
54
55 164 values of z_{\max} , because the difference in the depth of the habitable layer (forced by surface
56
57 165 temperature) corresponds to a larger shift towards the star. However, the asymptote in the depth
58
59
60
61
62
63
64
65

1
2
3
4 166 of the habitable layer is determined where solar irradiation approaches zero and is therefore
5
6
7 167 independent of albedo.

8
9
10 168

11 12 13 169 *3.2. Effect of planetary size*

14
15
16
17 170 Planetary masses (M) $0.1 - 10 \times$ Earth-mass (M_{\oplus}) were modelled, with bulk density and heat
18
19 171 production per unit mass held constant at bulk-Earth values. Larger radii generate steeper
20
21
22 172 geothermal gradients and proportionally shallower and thinner habitable layers less sensitive to
23
24 173 solar radiation (**Figure 3**). For $M/M_{\oplus} = 10$, a habitable layer ~ 1.5 km thick is supported less than
25
26
27 174 6 km below the surface in interstellar space. However, if z_{\max} is related to a minimum threshold
28
29 175 in porosity or permeability (see *1.3*) then it must decrease with increasing lithostatic pressure,
30
31
32 176 which is proportional to gravitational field strength and hence planetary radius. Increasing the
33
34 177 planetary radius can therefore reduce both the depth of the habitable layer and z_{\max} at the same
35
36
37 178 rate, such that the SSHZ is unaffected. This result only applies when the internal heat flux
38
39 179 negligibly affects surface temperature; within the limits of Figure 2, it applies within ~ 7 AU.

40 41 42 180 *3.3. Application to Earth, Mars and exoplanets*

43
44
45
46 181 SSHZ outer edges for Earth, Mars and a selection of exoplanets are presented (**Table 1**). Mars
47
48 182 ($\sim 0.1 M_{\oplus}$) is approximated by the general (equilibrium) model. The habitable layer is found to
49
50
51 183 extend from 5.3 km to 14.0 km below the surface (unless limited by z_{\max}). A hypothetical Mars-
52
53 184 average-salinity melting point of -10 °C (Jones et al., 2011) raises the top of the habitable layer
54
55
56 185 to 4.5 km below the surface. These results are similar to other recent estimates (e.g. Clifford et
57
58 186 al., 2010) despite the use of Earth's heat production per unit mass.

1
2
3
4
5
6
7
8
9
10
11
12
13
14
15
16
17
18
19
20
21
22
23
24
25
26
27
28
29
30
31
32
33
34
35
36
37
38
39
40
41
42
43
44
45
46
47
48
49
50
51
52
53
54
55
56
57
58
59
60
61
62
63
64
65

187 For Earth, the model is adjusted to include some simple, temperature-dependent greenhouse gas
188 fluxes, as described in 2.1. These introduce sharp changes in surface temperature, and
189 consequently in the depth of the habitable layer, at both edges of the conventional HZ (**Figure**
190 **4**). For the most Earth-like case, the SSHZ is ~3 and ~14 times wider than the conventional HZ
191 for a biosphere shallower than 5 and 10 km respectively. In Earth’s present position, the average
192 base of the biosphere is predicted to occur at 2.8 km depth, corresponding to a predicted average
193 thermal conductivity of $\sim 2.3 \text{ W m}^{-1} \text{ K}^{-1}$.

194 Four low-mass super-earths were selected for investigation based on their low mass and variety
195 of positions with respect to the surface HZ (Schneider, 2010; Vogt et al., 2010). As in the
196 calculation of conventional (surface) habitable zones, an Earth-like atmosphere is assumed (see
197 2.1); we also assume Earth values for bulk density and heat production per unit mass. Since these
198 assumptions are only partially valid, the results are best regarded as illustrative. HD 85512 b is
199 outside the inner edge of the conventional HZ ($T_s = 181 \text{ }^\circ\text{C}$), Gliese 667 Cc lies within the
200 conventional HZ but close to the inner edge ($T_s = 75 \text{ }^\circ\text{C}$), Gliese 581g (unconfirmed; $T_s = -11$
201 $^\circ\text{C}$) is just beyond the outer edge; and Gliese 581 d is far beyond the outer edge ($T_s = -84 \text{ }^\circ\text{C}$).
202 However, all but HD 85512 b, which cannot support liquid water at any depth, are found to lie
203 within the SSHZ for 2 km depth, i.e., they possess temperatures suitable for liquid water less
204 than 2 km below the surface.

4. Discussion

4.1 Uncertainties and limitations

207 To constrain both HZs and SSHZs for real planetary bodies requires modelling of surface
208 temperature based on incoming solar radiation, atmospheric composition, and (bio)geochemical

1
2
3
4
5
6
7
8
9
10
11
12
13
14
15
16
17
18
19
20
21
22
23
24
25
26
27
28
29
30
31
32
33
34
35
36
37
38
39
40
41
42
43
44
45
46
47
48
49
50
51
52
53
54
55
56
57
58
59
60
61
62
63
64
65

209 feedbacks. For SSHZs, additional modelling is required to estimate heat production, transport
210 and loss due to accretion, radioactive decay, tidal and other gravitational effects in planets of
211 different compositions, sizes, ages, and tectonic regimes. Small terrestrial planets without surface
212 liquid water probably cannot support plate tectonics and should therefore lose internal heat less
213 efficiently than the Earth. Nevertheless, the present model yields both an appropriate geotherm
214 for Earth and a Mars geotherm similar to those of other studies (e.g. Clifford et al. 2010).

215 The age and hence accretional heat reserves of exoplanets of known mass might be very broadly
216 constrained by the spectroscopic and activity profiles of their host stars (Lachaume et al., 1999).
217 Planetary radiogenic heat production depends on both age and the initial abundance of
218 radioactive isotopes of U, Th and K. 70 – 90% of stars surveyed formed in clusters within gas or
219 dust clouds; 75% of these clusters contain massive stars, implying a high likelihood of
220 contamination by supernova explosions (Lada and Lada, 2003). While U/O and Th/O ratios
221 should be relatively constant for planets forming within 10 Ga of a supernova explosion, K
222 enrichments may be more variable (Valencia et al., 2007).

223 Both conventional HZs and SSHZs are necessarily based on global average temperatures despite
224 the potential for large regional variations and for habitable micro-habitats on broadly hostile
225 planets (Nisbet et al. 2007). Deeper and shallower habitable regions can result from variations in
226 connected pore space, nutrient and energy availability and heat flux, the latter expressing
227 latitude, climate, composition, geodynamic processes, and impact events. On Mars, for example,
228 localised convection cells may carry liquid water in aquifers several km above the background
229 T_{min} isotherm (Travis et al., 2003), and seasonal surface features have been tentatively interpreted
230 as briny flows (McEwen et al., 2011).

1
2
3
4
5
6
7
8
9
10
11
12
13
14
15
16
17
18
19
20
21
22
23
24
25
26
27
28
29
30
31
32
33
34
35
36
37
38
39
40
41
42
43
44
45
46
47
48
49
50
51
52
53
54
55
56
57
58
59
60
61
62
63
64
65

231 On Earth, the thick continental crust supports a gentler geothermal gradient than the thin basaltic
232 oceanic crust. Our model predicts that Earth’s biosphere should extend on average 2.8 km below
233 the surface. This may be a reasonable average across Earth’s two crustal types, although data for
234 comparison are sparse. Prokaryotes have been found in the oceanic crust at 1.6 km depth and
235 ~100 °C (Mason et al., 2010). On the continents, the three deepest boreholes searched for life (to
236 the authors’ knowledge) have yielded, respectively, living organisms at 3.6 km (48 °C) and 5.3
237 km (70 °C) and sterile waters at 4 km depth (110 °C) (Szewzyk et al., 1994; Borgonie et al.,
238 2011; Huber et al., 1994). Substituting the higher conductivity of continental crust into our
239 model predicts an average continental biosphere thickness of ~4 km.

240 We have not considered the effects of impurities (e.g. ammonia) and ultra-high pressures on the
241 phase transitions of water. Lower values of T_{\min} than 0 °C can be considered for impure water,
242 raising the top of the habitable layer and expanding the SSHZ. Cell growth has been reported at
243 -20 °C (Canganella and Wiegel, 2007); however, we regard liquid water as essential for
244 habitability. The choice of 122 °C as T_{\max} might be made obsolete by future studies of
245 thermophiles. Raising T_{\max} lowers the base of the habitable layer but does not affect SSHZ outer
246 edge positions.

247 *4. 2 Adaptation to icy bodies*

248 Icy bodies are of particular interest because SSHZs extend much further than solar system frost
249 lines, beyond which planetary bodies are volatile-rich. We note that our model for terrestrial
250 planets could be adapted to find SSHZs for icy bodies by treating sub-ice oceans as habitable
251 layers. For instance, treating Titan as a shell of pure water/ice around a heat-generating core
252 (Grasset et al., 2000) and accounting for the pressure-dependent melting point and temperature-
253 dependent thermal conductivity of water ice (Chizhov, 1993; Petrenko and Whitworth, 1999), we

1
2
3
4
5
6
7
8
9
10
11
12
13
14
15
16
17
18
19
20
21
22
23
24
25
26
27
28
29
30
31
32
33
34
35
36
37
38
39
40
41
42
43
44
45
46
47
48
49
50
51
52
53
54
55
56
57
58
59
60
61
62
63
64
65

254 obtain an ice thickness of ~85 km at Titan’s present position and an SSHZ outer edge of ~1 AU
255 for 10 km depth. A sophisticated treatment of the internal structure of icy bodies is beyond our
256 purposes here but should take account of: (a) convection, and (b) the effects of clathrates,
257 impurities (notably ammonia) and high-pressure ice phases on thermal conductivity and melting
258 points. The forthcoming ESA JUICE mission should determine useful information about these
259 parameters and direct measurements of ice-thickness for Ganymede, Europa and Callisto
260 (Dougherty et al., 2011). However, it is doubtful whether circumstellar habitable zones are
261 appropriate tools for locating habitable icy moons, whose dominant heat source may be tidal
262 rather than solar energy.

263

264 *4.3 Conclusions*

265 The example of our own solar system suggests that most planets in the universe are beyond the
266 outer edge of conventional surface habitable zones, although exoplanets closer to their stars are
267 easier to detect. Moreover, surface habitability may commonly be precluded by ionizing solar
268 and cosmic radiation, especially under thin atmospheres and weak geomagnetic fields; or by
269 corrosive atmospheres, while the subsurface is insulated from these hazards by layers of rock
270 (Fisk and Giovannoni, 1998; Dartnell et al., 2007). Besides a favourable temperature, pressure
271 and radiation environment, life requires long-term nutrient and energy supplies. Subsurface
272 environments in both rocky and icy bodies are likely to meet these requirements for at least low
273 levels of biological activity while partially or even completely isolated from surface (Gaidos et
274 al., 1999; Lin et al., 2006; Sleep, 2012). These considerations, together with our results, suggest
275 that habitable environments may occur much more commonly deep within planets and moons
276 than on their surfaces. Deeper biospheres are probably much less likely to produce planetary

1
2
3
4
5
6
7
8
9
10
11
12
13
14
15
16
17
18
19
20
21
22
23
24
25
26
27
28
29
30
31
32
33
34
35
36
37
38
39
40
41
42
43
44
45
46
47
48
49
50
51
52
53
54
55
56
57
58
59
60
61
62
63
64
65

277 biosignatures amenable to remote sensing, although potential search targets include atmospheric
278 chemistry, cryovolcanic plume chemistry (McKay et al., 2008), and the compositions of
279 hydrothermal and cryovolcanic surface residues. However, if life can originate in the subsurface
280 of cold planets, then the probability of detecting a deep biosphere on a randomly selected
281 terrestrial planet might be comparable to the probability of detecting a (more readily apparent but
282 rarer) surface biosphere.

283

1
2
3
4
5
6
7
8
9
10
11
12
13
14
15
16
17
18
19
20
21
22
23
24
25
26
27
28
29
30
31
32
33
34
35
36
37
38
39
40
41
42
43
44
45
46
47
48
49
50
51
52
53
54
55
56
57
58
59
60
61
62
63
64
65

284 **Acknowledgements**

285 SM and JOJ are grateful to the UK Science and Technology Facilities Council (STFC) for
286 Aurora Studentships. We thank Dr. Stephen Clifford (LPI), Dr. Ravi Kopparapu (Penn State),
287 and Claire Davis (St. Andrews) for generous technical advice. We thank Norm Sleep and two
288 anonymous reviewers for constructive reviews of the manuscript.

References

Borgonie, G. et al., 2011. Nematoda from the terrestrial deep subsurface of South Africa. *Nature* 474, 79–82.

Boston, P.J., Ivanov, M.V., & McKay, C.P., 1992. On the possibility of chemosynthetic ecosystems in subsurface habitats on Mars. *Icarus* 95, 300–308.

Caldeira, K., & Kasting, J. F., 1992. Susceptibility of the early earth to irreversible glaciation caused by carbon dioxide clouds. *Nature* 359, 226–228.

Canganella, F., & Wiegel, J., 2011. Extremophiles: From abyssal to terrestrial ecosystems and possibly beyond. *Naturwissenschaften* 4 , 253–279.

Chizhov, V., 1993. Thermodynamic properties and thermal equations of the state of high-pressure ice phases. *Journal of Applied Mechanics and Technical Physics* 34, 253–262.

Clauser, C., & Huenges, E., 1995. Thermal Conductivity of Rocks and Minerals, in: T. J. Ahrens (Ed.), *Rock Physics and Phase Relations - a Handbook of Physical Constants*, AGU Reference Shelf, Vol. 3, American Geophysical Union, pp. 105–126.

- 1
2
3
4 Clifford, S. M. et al., 2010. Depth of the Martian cryosphere: Revised estimates and implications
5
6 for the existence and detection of subpermafrost groundwater. *J. Geophys. Res.* 115, E07001.
7
8
9
10 Dartnell, L., Desorgher, L., Ward, J., & Coates, A., 2007. Martian sub-surface ionising radiation:
11
12 Biosignatures and geology. *Biogeosciences Discussions* 4, 455–492.
13
14
15
16 Dougherty, M., et al., 2011. JUICE: Exploring the emergence of habitable worlds around gas
17
18 giants. ESA Assessment Study Report ESA/SRE(2011)18 (Yellow Book).
19
20
21
22 Fisk, M. R., & Giovannoni, S. J., 1999. Sources of nutrients and energy for a deep biosphere on
23
24 Mars. *J. Geophys. Res.* 104, 11805–11815.
25
26
27
28 Gaidos, E. J., Neelson, K. H., & Kirschvink, J. L., 1999. Life in ice-covered oceans. *Science* 284,
29
30 1631–1633.
31
32
33
34 Gold, T., 1992. The deep, hot biosphere. *Proc. Natl. Acad. Sci. USA* 89, 6045–6049.
35
36
37
38 Grasset, O., Sotin, C., & Deschamps, F., 2000. On the internal structure and dynamics of Titan.
39
40 *Planet. Space Sci.* 48, 617–636.
41
42
43
44 Huber, H. Huber, R., Ludemann, H. & Stetter, K. O., 1994. Search for hyperthermophilic
45
46 microorganisms in fluids obtained from the KTB pump test. *Scientific Drilling* 4, 127–129.
47
48
49
50 Jones, E. G., Lineweaver, C. H., & Clarke, J. D., 2011. An extensive phase space for the
51
52 potential martian biosphere. *Astrobiology* 11, 1017–1033.
53
54
55
56 Kasting, J. F., Whitmire, D. P., & Reynolds, R. T., 1993. Habitable zones around main sequence
57
58 stars. *Icarus* 101, 108–128.
59
60
61
62
63
64
65

- 1
2
3
4 Kopparapu, R. K. et al., 2013. Habitable zones around main-sequence stars: new estimates.
5
6
7 *Astrophys. J.* (Accepted). arXiv:1301.6674
8
9
10 Lachaume, R., Dominik, C., Lanz, T., & Habing, H., 1999. Age determinations of main-
11
12 sequence stars: Combining different methods. *Astronomy and Astrophysics* 348, 897–909.
13
14
15
16 Lada, C. J., & Lada, E. A., 2003. Embedded clusters in molecular clouds. *Astronomy and*
17
18 *Astrophysics* 41, 57–115.
19
20
21
22 Lin, L. H., Slater, G. F., Sherwood Lollar, B., Lacrampe-Couloume, G., & Onstott, T., 2005. The
23
24 yield and isotopic composition of radiolytic H₂, a potential energy source for the deep subsurface
25
26 biosphere. *Geochimica Et Cosmochimica Acta* 69, 893–903.
27
28
29
30 Lin, L. et al., 2006. Long-term Sustainability of a High-Energy, Low-Diversity Crustal Biome.
31
32 *Science* 314, 479–482.
33
34
35
36 Mason, O. U. et al., 2010. First investigation of the microbiology of the deepest layer of ocean
37
38 crust. *PloS One* 5, e15399.
39
40
41
42 McEwen et al., 2011. Seasonal flows on warm martian slopes. *Science* 333, 740-743.
43
44
45
46 McKay, C. P., Porco, C. C., Altheide, T., Davis, W. L., & Kral, T. A., 2008. The possible origin
47
48 and persistence of life on Enceladus and detection of biomarkers in the plume. *Astrobiology* 8,
49
50 909–919.
51
52
53
54 Nisbet, E. et al., 2007. Creating Habitable Zones, at all Scales, from Planets to Mud Micro-
55
56 Habitats, on Earth and on Mars. *Space Sci. Rev.* 129, 79–121.
57
58
59
60
61
62
63
64
65

- 1
2
3
4 Petrenko, V. F., & Whitworth, R. W., 1999. *Physics of Ice*, Clarendon Press, Oxford.
5
6
7
8 Pollack, H. N., Hurter, S. J., & Johnson, J. R., 1993. Heat flow from the earth's interior: Analysis
9
10 of the global data set. *Rev. Geophysics* 31, 267–280.
11
12
13
14 Raulin, F., Hand, K. P., McKay, C. P., Viso, M., 2010. Exobiology and Planetary Protection of
15
16 icy moons. *Space Sci. Rev.* 153, 511–535.
17
18
19
20 Roussel, E. G., Bonavita, M. C., Querellou, J., Cragg, B. A., & Webster, G., 2008. Extending the
21
22 sub-sea-floor biosphere. *Science* 320, 1046.
23
24
25
26 Schneider, J., 2010. *The Extrasolar Planets Encyclopaedia*. <http://exoplanet.eu>.
27
28
29
30 Selsis, F. et al., 2008. Habitable planets around the star GL 581? *Astronomy & Astrophysics*
31
32 476, 1373–1387.
33
34
35
36 Sharma, A. et al., 2002. Microbial activity at gigapascal pressures. *Science* 295, 1514–1516.
37
38
39
40 Sleep, N. H., 2012. Maintenance of permeable habitable subsurface environments by earthquakes
41
42 and tidal stresses. *Int. J. Astrobiol.* 11, 257–268.
43
44
45
46 Szewzyk, U., Szewzyk, R., & Stenström, T. A., 1994. Thermophilic, anaerobic bacteria isolated
47
48 from a deep borehole in granite in sweden. *PNAS* 91, 1810–1813.
49
50
51
52 Takai, K. et al., 2008. Cell proliferation at 122 C and isotopically heavy CH₄ production by a
53
54 hyperthermophilic methanogen under high-pressure cultivation. *PNAS* 105, 10949–10954.
55
56
57
58 Travis, B. J., Rosenberg, N. D., & Cuzzi, J. N., 2003. On the role of widespread subsurface
59
60 convection in bringing liquid water close to mars' surface. *J. Geophys. Res.* 108, 10.1029.

1
2
3
4 Valencia, D., O'Connell, R. J., & Sasselov, D. D., 2007. Inevitability of plate tectonics on super-
5
6 earths. *Astrophys. J. Lett.* 670, L45–L48.
7
8

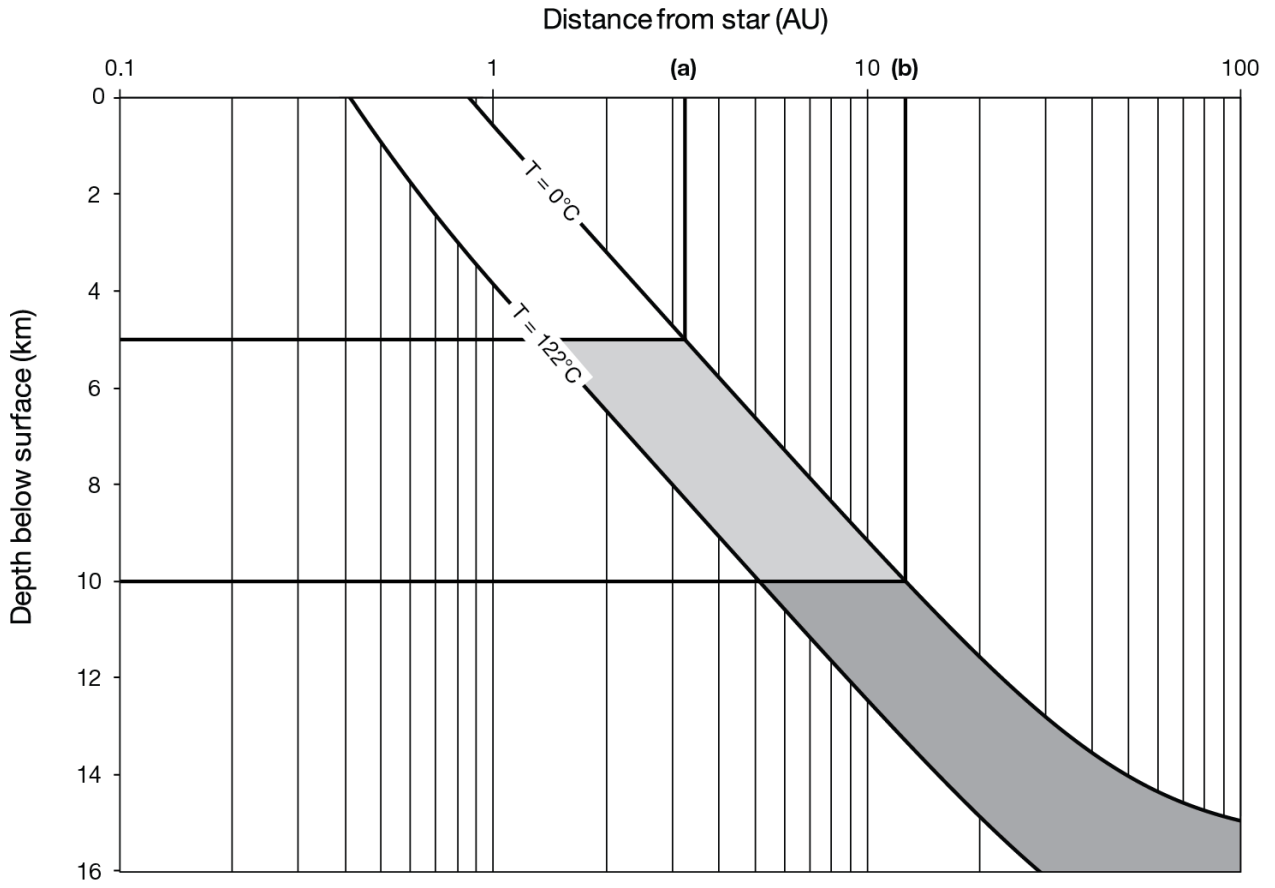
9
10 Vanlint, D., Mitchell, R., Bailey, E., Meersman, F., McMillan, P. F., Michiels, C. W., & Aertsen,
11
12 A., 2011. Rapid acquisition of Gigapascal-High-Pressure Resistance by *Escherichia coli*. *mBio*
13
14 2, e00130-10.
15
16
17

18 Vogt, S. S., Butler, R. P., Rivera, E. J., Haghighipour, N., Henry, G. W., & Williamson, M. H.,
19
20 2010. The Lick-Carnegie exoplanet survey: A 3.1 M_⊕ planet in the habitable zone of the nearby
21
22 M3V star Gliese 581. *Astrophys. J.* arXiv:1009.5733.
23
24
25

26 Whitman, W. B., Coleman, D. C., & Wiebe, W. J., 1998. Prokaryotes: the unseen majority.
27
28 *PNAS* 95, 6578–6583.
29
30
31

1
2
3
4
5
6
7
8
9
10
11
12
13
14
15
16
17
18
19
20
21
22
23
24
25
26
27
28
29
30
31
32
33
34
35
36
37
38
39
40
41
42
43
44
45
46
47
48
49
50
51
52
53
54
55
56
57
58
59
60
61
62
63
64
65

290 **FIGURE 1**

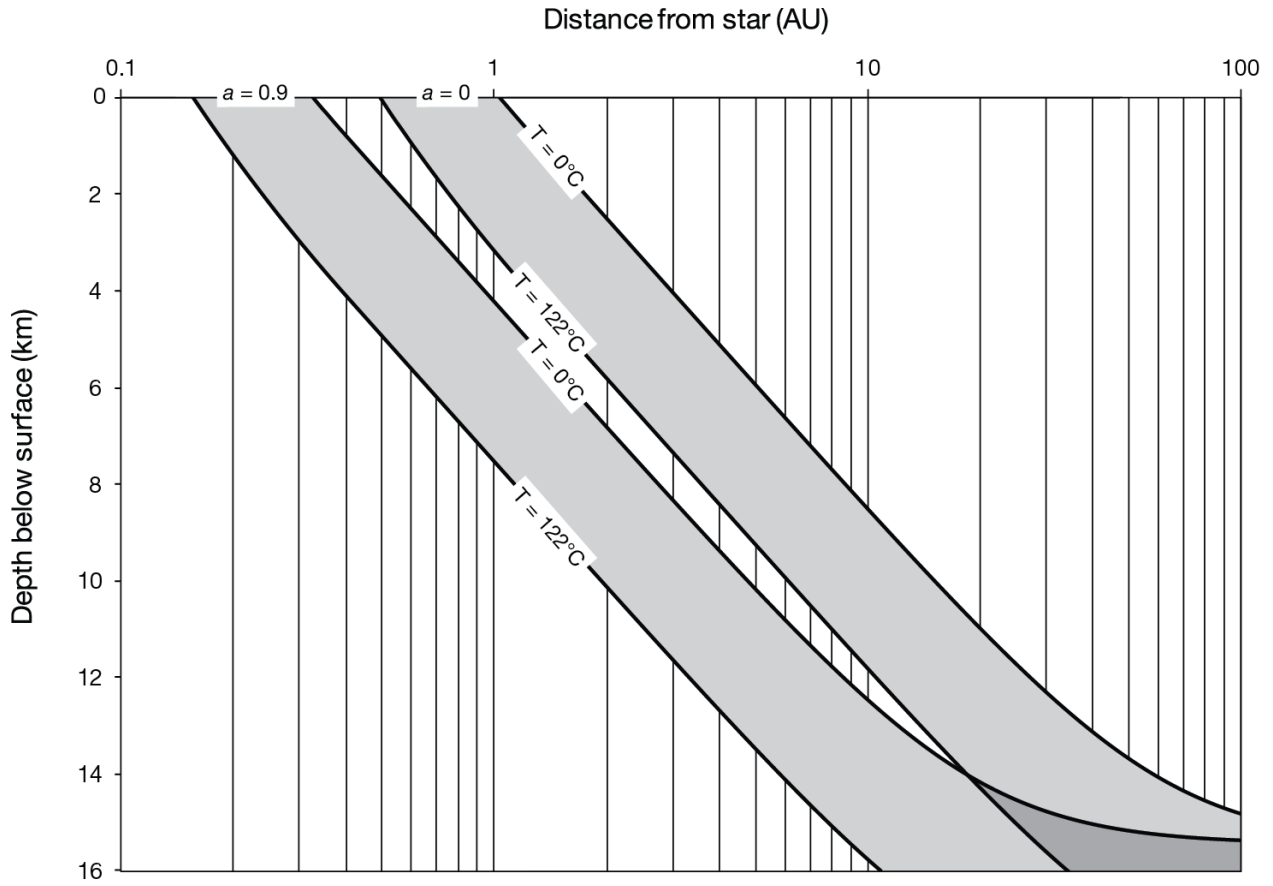


291

292 **Figure 1. Circumstellar subsurface-habitability zones (SSHZ).** Habitable layers and SSHZ
293 outer edges for two values of z_{\max} , a stipulated maximum habitable depth (where a planet within
294 the SSHZ for $z_{\max} = x$ can sustain liquid water at some depth $\leq x$). For $z_{\max} = 5$ km, the outer edge
295 of the SSHZ **(a)** falls at 3.2 AU; for $z_{\max} = 10$ km, the outer edge **(b)** falls at 12.6 AU. The outer-
296 edge position tends to infinity as z_{\max} approaches about 15.42 km. Calculations assume the
297 Earth's current size, bulk density, heat production per unit mass, albedo and emissivity.

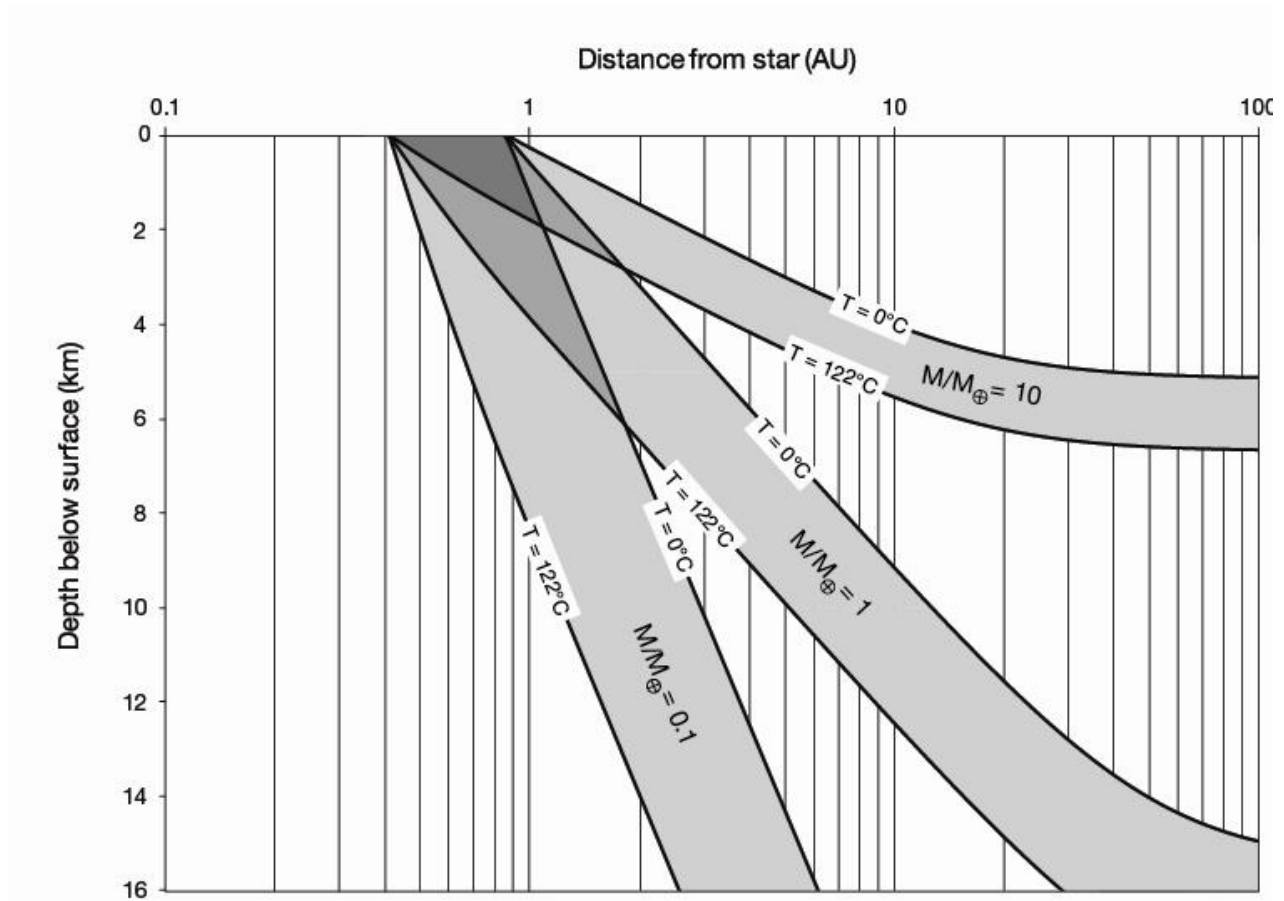
298

1
2
3
4 **FIGURE 2**
5
6
7



300 **Figure 2. The relationship between subsurface habitability and surface albedo. Top**
301 Habitable-layer depth as a function of heliocentric distance for two extremes of planetary Bond
302 albedo (a). For $a = 0.9$, the SSHZ is narrower and closer to the star than for $a = 0$. Calculations
303 assume the Earth's current size, bulk density, heat production per unit mass and emissivity.

1
2
3
4
5
6
7
8 **FIGURE 3**
9

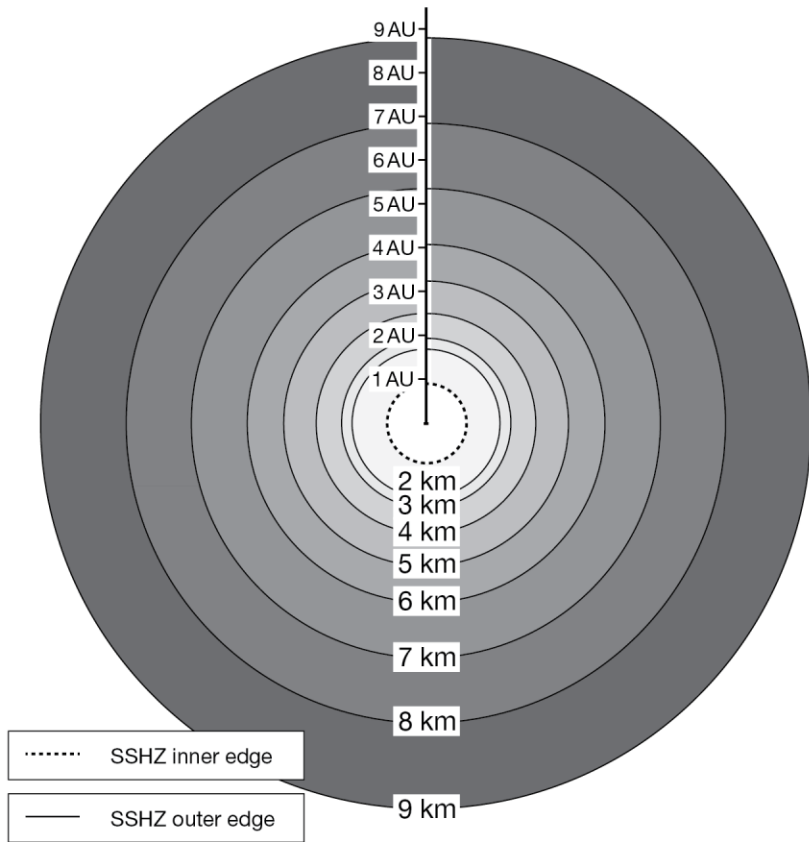
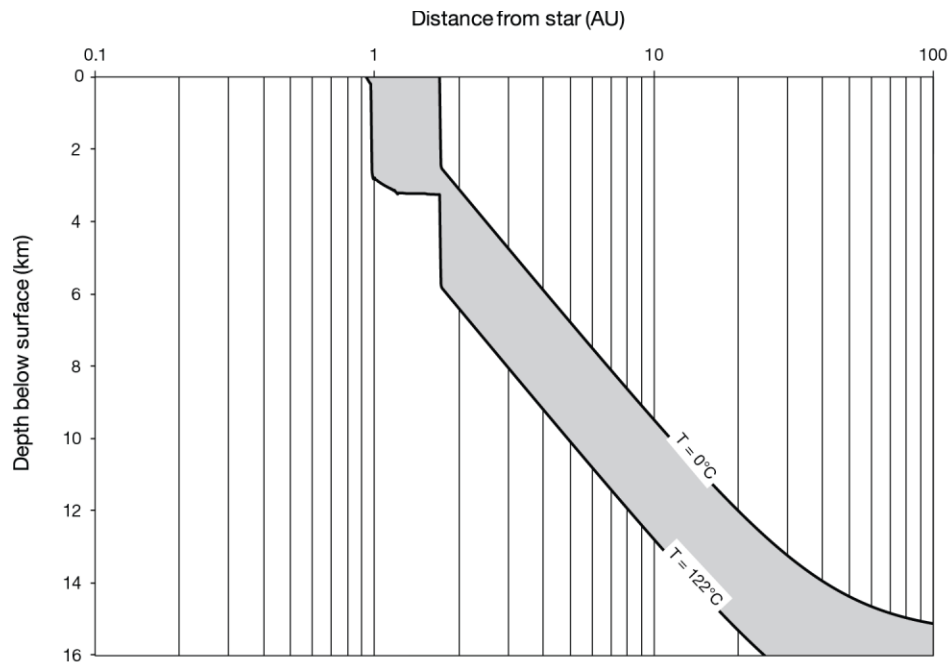


43 **Figure 3. Habitable layers for three planetary masses.** M_{\oplus} = Earth-mass. The differences in
44
45
46
47
48
49
50
51
52
53
54
55
56
57
58
59
60
61
62
63
64
65

304 **Figure 3. Habitable layers for three planetary masses.** M_{\oplus} = Earth-mass. The differences in
305 internal heat production are insufficient to shift significantly the position of the surface HZ but
306 become significant in the subsurface. Consequently, subsurface habitable layers are thinner,
307 shallower and less sensitive to the solar heat flux for larger planets. Calculations assume the
308 Earth's bulk density, heat production per unit mass, albedo and emissivity.

1
2
3
4
5
6
7
8
9
10
11
12
13
14
15
16
17
18
19
20
21
22
23
24
25
26
27
28
29
30
31
32
33
34
35
36
37
38
39
40
41
42
43
44
45
46
47
48
49
50
51
52
53
54
55
56
57
58
59
60
61
62
63
64
65

311 **FIGURE 4**



1
2
3
4
5
6
7
8
9
10
11
12
13
14
15
16
17
18
19
20
21
22
23
24
25
26
27
28
29
30
31
32
33
34
35
36
37
38
39
40
41
42
43
44
45
46
47
48
49
50
51
52
53
54
55
56
57
58
59
60
61
62
63
64
65

312 **Figure 4. Circumstellar subsurface-habitability zones (SSHZ) for a deep biosphere on an**
313 **Earth-like planet.** **Top:** The depth of a habitable layer on an Earth-like planet as a function of
314 orbital distance. Sharp downward steps indicate greenhouse feedbacks in the atmosphere model.
315 **Below:** The same model output represented as SSHZ outer edges in the first 10 AU at 1 km
316 intervals of z_{max} , the maximum habitable depth (where a planet within the SSHZ for $z_{max} = x$ can
317 sustain liquid water at some depth $\leq x$). Calculations assume the Earth's current size, bulk
318 density and heat production per unit mass, so should be regarded as illustrative.

TABLE 1

319 Estimated circumstellar subsurface-habitability zone (SSHZ) outer edges for selected
320 planetary bodies. SSHZ outer edges are shown for an appropriate range of maximum habitable
321 depths, z_{\max} (such that any planet within a SSHZ for $z_{\max} = x$ can sustain liquid water at some
**322 depth $\leq x$). Subscript \oplus denotes Earth. Orbital distances are semi-major axes. $M =$ mass. $\rho =$
**323 density. $a =$ albedo. $T_s =$ surface temperature. $*$ = at semi-major axis orbital distance. Gliese 581
**324 g is unconfirmed. $\dagger =$ minimum mass. Calculations for Earth and exoplanets use Earth’s bulk
**325 density and an Earth-like atmosphere model; all calculations use Earth’s heat production per unit
326 mass.********

Planetary body					Model results					
Terrestrial planet	Orbital distance (AU)	—	—	a	T_s^* (°C)	Habitable layer top (km)*	SSHZ outer edge (AU) for $z_{\max} =$			
							4 km	8 km	16 km	32 km
Earth	1	1	1	N/A	+15	0	2.5	7.3	∞	∞
Mars	1.5	0.1	0.7	0.25	-62	5.3	1.3	2.0	4.5	23
Mars (10% salinity)	1.5	0.1	0.7	0.25	-62	4.5	1.4	2.2	4.9	25
Exoplanet	Stellar luminosity / Solar	Orbital distance (AU)		—	T_s^* (°C)	Habitable layer top (km)*	SSHZ outer edge (AU) for $z_{\max} =$			
							1 km	2 km	4 km	8 km
Gliese 581 d	0.013	0.218	5.6	-84	1.6	0.17	0.27	0.64	∞	
Gliese 581 g (U)	0.013	0.140	3.1	-11	0.21	0.16	0.23	0.46	2.4	
HD 85512 b	0.126	0.26	3.6	+181	N/A	0.49	0.71	1.5	10.7	
Gliese 667 Cc	0.0137	0.123	4.5	+75	0	0.18	0.25	0.57	∞	

Figure 1

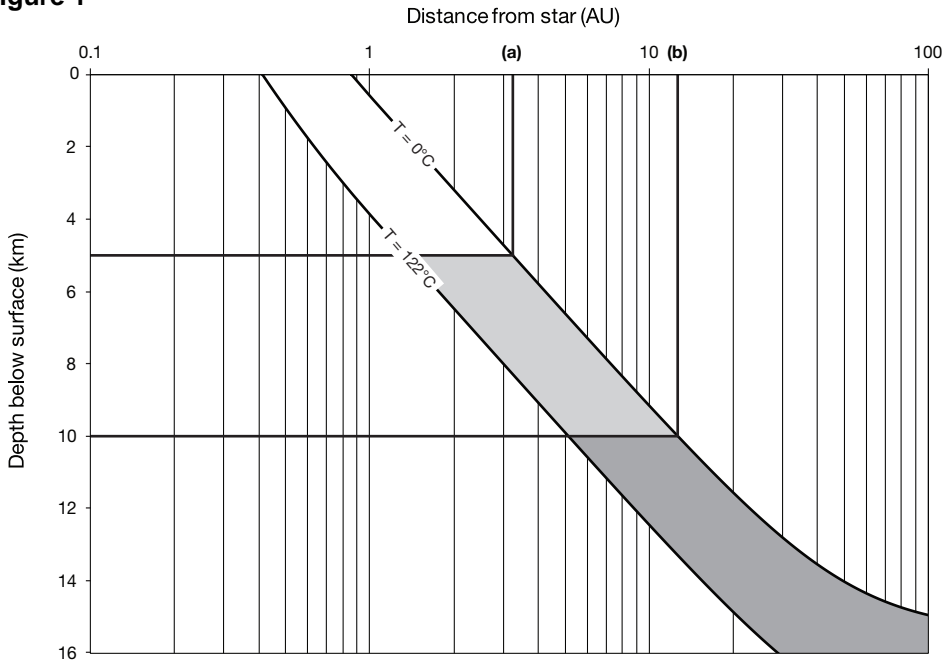


Figure 2

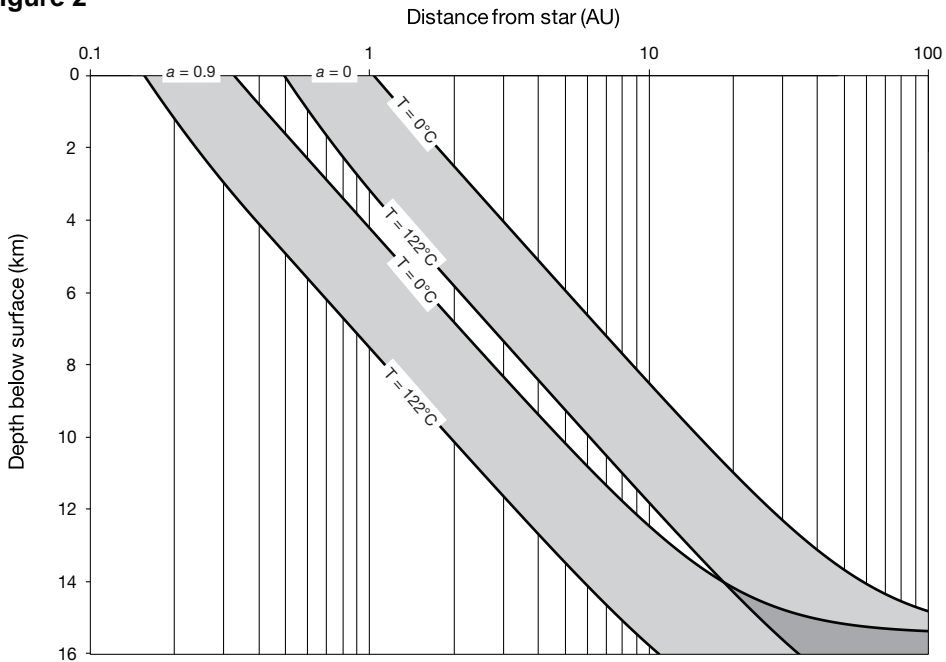


Figure 3

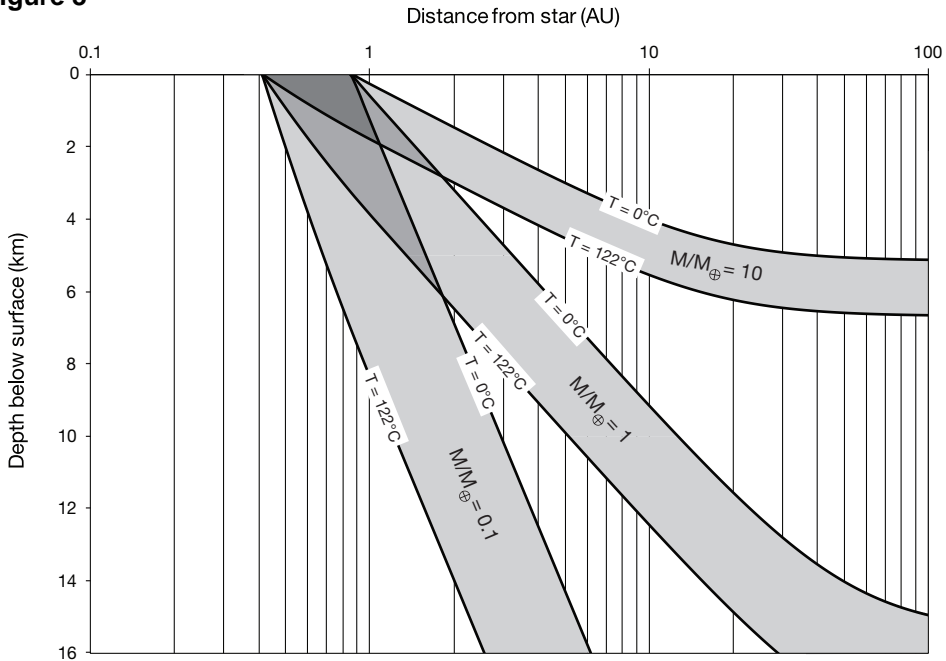


Figure 4

